This article has been accepted for publication in a future issue of this journal, but has not been fully edited. Content may change prior to final publication. Citation information: DOI 10.1109/TIM.2019.2950612, IEEE Transactions on Instrumentation and Measurement

Methods to Estimate Gas Attenuation in Absence of a Radiometer to Support Satellite Propagation Experiments

Lorenzo Luini, *Senior Member, IEEE,* Gustavo A. Siles, *Member, IEEE,*
José Manuel Riera, *Senior Member, IEEE,* Carlo Riva, *Senior Member, IEEE,* and James Nessel

***Abstract*— The experimental characterization of tropospheric effects on electromagnetic waves relies on the reception of a beacon signal transmitted by a satellite. The total tropospheric attenuation can be derived from these measurements in combination with additional information, specifically the attenuation due to atmospheric gases, in turn derived from ancillary instruments or data sources. When available, this information is obtained from a co-sited radiometer. This paper presents three alternative procedures to estimate the gas attenuation that can be used in the absence of this instrument: the first one makes use of zenith total delay data obtained from GNSS (Global Navigation Satellite System) receivers and additional meteorological data, the second one relies on atmospheric profiles gathered from radiosonde observations and/or NWP (Numerical Weather Prediction) products and the third one only makes use of standard atmospheric profiles. The accuracy of the procedures when used in this application is compared with the reference total tropospheric attenuation derived with the support of radiometric data, exploiting the Alphasat beacon measurements collected in Milan, Italy, in 2017. The results indicate that a better accuracy (average *RMS* error below 0.1 dB when compared with the use of a radiometer) is achieved by using GNSS data because of their finer temporal resolution; nonetheless, the three procedures can be equally recommended, their use being conditioned to the availability of the appropriate data in the area around the experimental site.**

Manuscript received June, XX, 2019. This work was supported in part by the Ministry of Science, Innovation and Universities of Spain through the RTI2018-098189-B-I00 project.. This work was also supported in part by the Air Force Office of Scientific Research, Air Force Material Command, USAF under Grant FA8655-13-1-3081.

L. Luini and C. Riva are with Politecnico di Milano, Milan, Italy, and with Consiglio Nazionale delle Ricerche, Milan, Italy (e-mail: lorenzo.luini@polimi.it).

G. A. Siles is with Universidad Privada Boliviana (UPB), Cochabamba, Bolivia (e-mail: gustavo.siles@upb.edu).

J. M. Riera is with Universidad Politécnica de Madrid (UPM), Madrid, Spain (e-mail: jm.riera@upm.es).

James Nessel is with NASA Glenn Research Center, Cleveland OH, USA (e-mail: james.a.nessel@nasa.gov).

Color versions of one or more of the Figs. in this communication are available online at http://ieeexplore.ieee.org.

Digital Object Identifier 10.1109/TAP.2016.xxx).

***Index Terms*— Satellite communication, millimeter-wave propagation, propagation measurements.**

I. Introduction

Satellite communications require wider and wider bandwidths to cope with the demand for new services with high throughput. The use of Ka-band frequencies is rapidly becoming more and more common [1], and will be supplemented in the next few years with the Q/V band portions of the spectrum [2] and, in a longer term, the W band [3]. Notwithstanding the benefits associated with the use of millimeter waves, they are seriously affected by propagation effects that take place in the troposphere leading to a variable attenuation level.

Propagation experiments designed to characterize these effects usually rely on the reception on the ground of a beacon continuous-wave unmodulated signal transmitted by a dedicated satellite using specialized receivers [4]-[5]. These experiments have been carried out in the past with the Olympus [6], Italsat [7] and ACTS [8] satellites, among others. The Alphasat satellite currently [9] provides the opportunity to implement experiments in the Ka and Q bands in Europe [10], and W-band experiments are under development [11]. These experiments require the simultaneous collection of meteorological data [12], which allow the atmospheric conditions to be characterized and the propagation parameters estimated, such as the tropospheric attenuation.

Additional information as regards the status of the atmosphere is required to derive and characterize the attenuation induced by the troposphere from the satellite beacon power measurements. A co-sited radiometer can usually provide this information when available. A single-channel radiometer can be integrated with the beacon receiver, enabling measurements of tropospheric attenuation to be taken along the same path and frequency band [13]-[14] or, alternatively, a separate multi-channel radiometer can be used to derive the integrated contents of the water vapor and liquid water in the atmosphere [15]-[16], as well as the attenuation at the frequency of interest [17]. In any case, the use of a radiometer provides an accurate estimation of the attenuation caused by tropospheric gases and clouds along the path in the absence of rain [18].

The main drawback of this approach is that radiometers are expensive instruments that need to be adequately maintained and calibrated; therefore, they are not always available for propagation experiments. This paper presents three alternative procedures which help to derive the total tropospheric attenuation from slant-path beacon measurements in the absence of a radiometer. The procedure developed by UPM-UPB (Universidad Politécnica de Madrid, Spain - Universidad Privada Boliviana, Bolivia) mainly makes use of Tropospheric Zenith Total Delay data obtained from a free-access GNSS (Global Navigation Satellite Systems) receiver [19]-[20]. On the other hand, the procedure developed by PoliMi (Politecnico di Milano, Italy) relies on atmospheric profiles obtained either from radiosonde observations (RAOBs) or from Numerical Weather Prediction (NWP) products. In the absence of these kinds of data, the PoliMi procedure can still be applied in a simplified way, which makes use of standard atmospheric profiles [21]. The three procedures allow the gas attenuation under clear sky conditions, to be estimated which is then used to derive the tropospheric attenuation from the satellite beacon measurements. Since gas attenuation presents a high correlation for similar-altitude sites located up to tens of kilometers, GNSS data or atmospheric vertical profiles from locations at such distances from the experimental site can be successfully used to this end.

The radiometric data used in this context are restricted to those collected in rain-free conditions [17], and allow both gas attenuation and cloud attenuation to be calculated. On the other hand, the three proposed procedures only allow the gas attenuation to be estimated. Their application in the derivation of the tropospheric attenuation is slightly different, since cloud attenuation events must be given the same consideration as rain events. For this reason, the assessment of the methods must be made on the basis of the tropospheric attenuation results. Indeed, comparing the gas attenuation time series derived from these procedures with those obtained from radiometric data would not provide a comprehensive evaluation of their accuracy. Therefore, the performance of the procedures is tested against the time series of tropospheric attenuation obtained with the support of radiometric data, specifically by taking advantage of the Alphasat beacon receiver measurements collected at 19.7 and 39.4 GHz at PoliMi during 2017. A comparison analysis on error metrics and yearly statistics allows the three techniques to be evaluated.

From a comparative point of view, the proposed alternative methods do not need the deployment of an expensive radiometer. They are based on meteorological and navigation data that normally are more easily available to the research community. To the best of our knowledge, so far no alternative techniques have been proposed, so this paper can contribute to fill this gap.

Following this introduction, Section II gives an overview of the experimental data considered in this work. The theoretical framework to derive tropospheric attenuation from the beacon signal measurements is introduced in Section III. The procedure developed by UPM-UPB is described in Section IV, whereas Section V details the PoliMi procedures. The results of the testing activity using the Alphasat data collected in Milan are shown and compared in Section VI. Finally, Section VII draws some conclusions on this work.

II. Experimental Data

A. Beacon Receiver Data

The data used in this contribution are collected within the framework of the Alphasat Aldo Paraboni propagation experiment [10], which is supported by the Italian Space Agency (ASI), and implemented by the European Space Agency (ESA), to achieve a better understanding of the atmospheric propagation characteristics in the Ka and Q bands. The space segment of the experiment includes the Alphasat satellite, a geosynchronous satellite owned by Inmarsat (25° East orbital position), which also holds the Aldo Paraboni payload, featuring two continuous-wave beacons at 19.701 GHz and 39.402 GHz.

A receiving station is installed on the rooftop of a building in the main campus of Politecnico di Milano in Milan, Italy (latitude 45.48° N, longitude 9.23° E, altitude 137 m a.m.s.l.). As shown in Fig. 1, the experimental equipment, developed and owned by the NASA Glenn Research Center (GRC), includes two receivers sampling the received beacon power at 8 samples per second. The diameter of the receiving antennas is 1.2 m (Ka band) and 0.6 m (Q band), respectively, and both receivers are equipped with step motors to track the Alphasat satellite, whose orbit has a variable inclination angle, slowly drifting up to 3° with reference to the Equatorial plane (the average link elevation angle is 35.6°).

B. GNSS Data

The EUREF Permanent GNSS Network (EPN) [22] is an international organization whose main task is to maintain the ETRS89 (European Terrestrial Reference System) standard geodetic coordinate reference system. In order to carry out this task, a wide network has been established, made up of approximately 280 GNSS reference stations [23]. Among the products provided by the EPN stations, estimates of Tropospheric Zenith Total Delays *ZTD* (mm) are available with a temporal resolution of 1 hour, in the form of weekly files in SINEX_TRO format, uploaded to a free-access FTP server with a latency of about 4 weeks [24].

In the present work, data from the EPN Como station (45.80° N, 9.09° E, 292-m a.m.s.l., code site COMO00ITA) have been collected. This is the closest station available to the PoliMi premises: the distance between the two sites is about 37 km. A total of 53 files from 2017 (GPS weeks from 1930 to 1982) were downloaded, and in-house software routines were implemented to extract *ZTD* estimates from each individual file. Missing data were identified corresponding to GPS week 1935 (February 5-11, 2017). Thus, zenith delay data from a total of 52 weekly files were finally used (data availability of 98%).

C. Meteorological Data

A variety of meteorological data have been exploited in this research work:

a) Surface meteorological data: 1 year (2017) of 1-minute measurements of atmospheric pressure, temperature and relative humidity collected at the PoliMi site. The availability is about 82% due to some outage periods (mainly August, but also some days in July and September).

b) Precipitation data: the rain intensity is measured at PoliMi site by a tipping bucket rain gauge and a laser-based disdrometer both operating at a 1-minute integration time, the latter also provides information on the drop size distribution and on the water phase (liquid, solid) of the hydrometeors. They are collocated by the Alphasat beacon receivers.

c) Radiosonde Observations (RAOBs): 3 years (2014-2016) of vertical profiles of pressure, temperature, and relative humidity, collected twice a day (0 and 12 UTC) at Milano Linate airport (45.26° N; 9.17° E; 122 m a.m.s.l., approximately 5 km from PoliMi site).

d) ECMWF (European Centre for Medium-range Weather Forecast) data: vertical profiles of pressure, temperature, and relative humidity, produced twice a day (0, 6, 12 and 18 UTC). The data are extracted from the analysis stage of the operational NWP products, which have 0.1°×0.1° latitude×longitude horizontal resolution and 137 vertical levels.

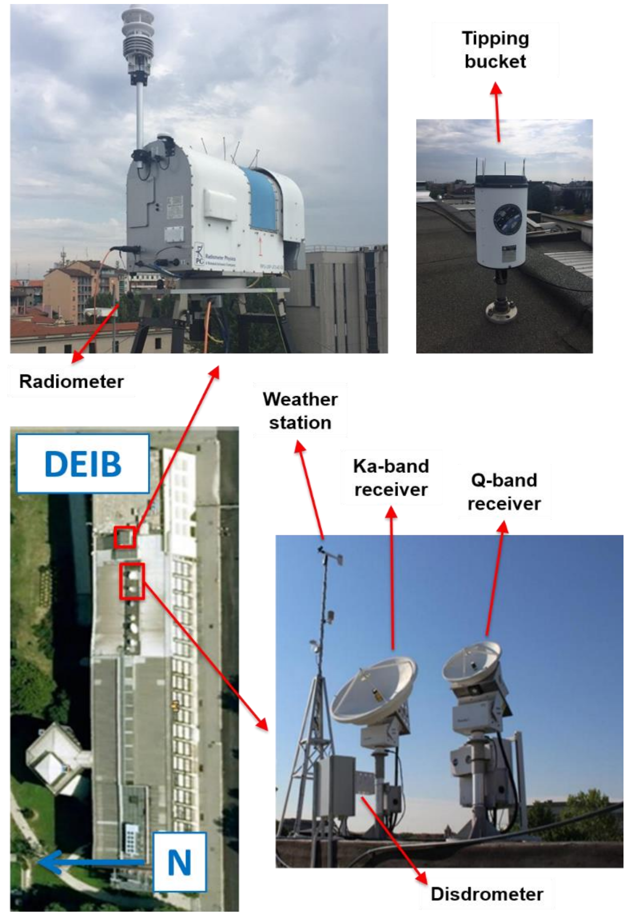

Fig. 1. NASA experimental equipment installed on the rooftop of the Dipartimento di Elettronica, Informazione e Bioingegneria (DEIB) of Politecnico di Milano. The 'N' box in the bottom left hand corner of the figure indicates the North direction.

D. Radiometric Data

A multi-channel radiometer, pointed along the path to the Alphasat satellite, supports the propagation experiment in Milan. Specifically, the instrument, manufactured by Radiometer Physics GmbH, measures the sky noise (also commonly referred to as the brightness temperature) at two channels in the Ka band (23.84 and 31.4) and two channels in the W band (72.5 and 82.5 GHz), which, in turn, is used to estimate the tropospheric attenuation in rain-free conditions using simple well-established algorithms [18].

III. Derivation of Tropospheric Attenuation from Propagation Measurements

In slant-path propagation experiments, the raw power P_r (dBm or dBW) received on the ground by a beacon receiver can be calculated as [25]:

$$P_r = EIRP - L_{bf} + G_{ant} + G_{rx} - A_g - A_c - A_r + A_{sc} \qquad (1)$$

The first four terms of (1) correspond to systematic components: satellite *EIRP* (dBm or dBW), free-space loss L_{bf} (dB), receiving antenna gain G_{ant} (dB) and receiver gain G_{rx} (dB). All of them can present variations in time. The satellite *EIRP* can change due to thermal variations within the satellite during the day. *EIRP* and L_{bf} can fluctuate due to orbital effects. G_{ant} can change due to depointing effects, if the satellite is not geo-stationary (as is the case of Alphasat, which is geosynchronous, with an orbit which has an inclination angle of up to 3º over the Equatorial plane), as well as thermal oscillations, although the latter are negligible in most cases. Finally, the changes in G_{rx} can mostly be related to thermal effects in the receiver. The changes in L_{bf} due to satellite range variations can be calculated and compensated, but the remaining effects are difficult to model with due precision. For this reason, the measurements must be referenced with a procedure ruling out the systematic factors.

The reference level P_{ref} (also typically referred to as 'template level') for tropospheric attenuation is defined as the signal power that would be received in the absence of the atmosphere, and can be expressed as the combination of the first four terms of (1), as shown in (2), with the result in the same units as *EIRP*:

$$P_{ref} = EIRP - L_{bf} + G_{ant} + G_{rx} \tag{2}$$

The variations in P_{ref} is usually slow, within 24-hour cycles, with some possible exceptions (for example, periods of satellite maneuvers). This means that P_{ref} can be evaluated for only part of the time, and interpolated for the rest, i.e. during atmospheric events.

The second group of four terms in (1) corresponds to different propagation effects and are expressed in dB: gas attenuation A_g (which is due to the absorption by water vapor and oxygen), cloud attenuation A_c and rain attenuation A_r (both A_c and A_r result from the electromagnetic scattering and absorption caused by cloud water droplets and rain drops, respectively), amplitude fluctuations due to tropospheric scintillation A_{sc} (which is induced by the presence of atmospheric turbulence along the link). The total tropospheric attenuation A (dB) is the sum of these four terms. Consequently, equation (1) can be re-written as:

$$P_r = P_{ref} - A \tag{3}$$

where the raw received power P_r and the reference level P_{ref} are in the same units (dBm or dBW). P_{ref} cannot be calculated directly from beacon measurements since some additional equipment is needed in order to estimate the four components of A and remove their effects from P_r.

The received power is averaged over tens or hundreds of seconds (typically 1 minute) in order to filter out the zero-mean scintillation component, and is expressed as $\overline{P_r}$. In the absence of rain attenuation, the reference level can be calculated as the combination of the averaged received power, plus gas and cloud attenuations:

$$P_{ref} = \overline{P_r} + A_g + A_c \tag{4}$$

This is the approach followed when a radiometer is available to measure both A_g and A_c. It is applied only in absence of rain, partially due to saturation effects in the measured brightness temperature, and partially to the complexity in solving the radiative transfer equation in presence of electromagnetic scattering [17],[18].

The alternative procedures presented in this paper provide the estimation only of the gas attenuation along the path, A_g; therefore, the reference power can be calculated in absence of rain attenuation and significant cloud attenuation, as:

$$P_{ref} = \overline{P_r} + A_g \tag{5}$$

In both procedures, the samples associated to rain and cloud events are discarded in the calculation of P_{ref}. In the UPM-UPB methodology, P_{ref} is later interpolated during rain and cloud events. The total tropospheric attenuation A (dB), including all propagation effects, is then calculated for all of the time with valid experimental data as:

$$A = P_{ref} - P_r \tag{6}$$

IV. UPM-UPB Procedure

Ground-based GNSS meteorology [26]-[27] is a sensing technique aimed at retrieving the Integrated Water Vapor *IWV* (mm) by analyzing the tropospheric delay in navigation signals [28]. The procedure developed by UPM-UPB aims to obtain A_g as the combination of the separate estimation of water vapor attenuation A_{wv} (dB) from *IWV*, and of dry air attenuation A_{dry} (dB) from surface temperature data. To this end, the method relies on the use of freely available tropospheric delay information provided by the GNSS networks, and to the vertical atmospheric profiles and surface meteorological registers. A noteworthy aspect of the use of GNSS data to estimate A_{wv} is that this technique is not influenced by the presence of liquid water particles in the atmosphere, either from clouds or rain, which is a valuable feature to be considered when this technique is compared with radiometric retrievals. Moreover, the input data need not be co-sited or from other locations in the area close the experimental site.

The procedure shares part of the steps described in [20], where A_g was used to validate time series of Ka-band tropospheric attenuation derived from a single-channel radiometer. However, in the present study, the application is different: the aim is to derive tropospheric attenuation at both Ka and Q bands from beacon measurements using A_g calculated by the procedure. Moreover, *ZTD* data were obtained in [20] from an IGS (International GNSS Service) station with a time resolution of 15 minutes, whereas in this paper they are extracted from the EPN Como station with a time resolution of 1 hour. Finally, the procedure implements additional steps aimed at compensating the effect of having a relevant height difference, which affects the retrieval of *IWV*. This important consideration was not taken into account in [20]. In the following subsections, the procedure is described and implemented using the GNSS and meteorological data described in Section II.

This article has been accepted for publication in a future issue of this journal, but has not been fully edited. Content may change prior to final publication. Citation information: DOI 10.1109/TIM.2019.2950612, IEEE Transactions on Instrumentation and Measurement

A. Calculation of A_{wv} from GNSS Data

The water vapor attenuation A_{wv} (dB) is related to the zenithal path with the value of IWV (mm) by the following expression:

$$A_{wv} = k_{wv} \cdot IWV \tag{7}$$

where k_{wv} (dB/mm) is the water vapor mass-absorption coefficient [17], which is frequency- and site-dependent. The values of 0.0119 dB/mm and 0.0105 dB/mm were derived, through least-square fitting [17], for k_{wv} at 19.7 and 39.4 GHz, respectively, using RAOBs from Milano Linate airport coupled with the line-by-line method in Annex 1 of Recommendation ITU-R P.676-11 [29].

The values of IWV in (7) are computed by exploiting the linear relationship with the Zenith Wet Delay ZWD (mm) given by [29]:

$$IWV = \frac{1}{c} \cdot ZWD \tag{8}$$

where:

$$ZWD = ZTD - ZHD \tag{9}$$

and

$$c = 10^{-6}\left(k_2' + \frac{k_3}{T_m}\right) R_w \cdot \rho_L \tag{10}$$

The set of parameters in (10) are as follows:

$$k_2' = k_2 - k_1 \cdot \varepsilon$$
$$k_1 = 77.689 \quad \mathrm{K \cdot hPa^{-1}}$$
$$k_2 = 71.295 \quad \mathrm{K \cdot hPa^{-1}}$$
$$\varepsilon = 0.622$$
$$k_3 = 3.754 \times 10^5 \quad \mathrm{K^2 \cdot hPa^{-1}}$$
$$R_w = 461.51 \ \mathrm{J \cdot kg^{-1}} \cdot K^{-1}$$
$$\rho_L = 1000 \quad \mathrm{kg} \cdot m^{-3}$$

where k_1, k_2 and k_3 are empirical refractive constants [30], ε is the ratio of the molar weight of water vapor M_w = 18.015 kg/kmol and the molar weight of dry air M_d = 28.964 kg/kmol, R_w is the specific gas constant for water vapor and ρ_L is the liquid water density. The mean temperature T_m is the average temperature of the atmosphere weighted by the partial pressure of water vapor e (in hPa) defined by:

$$T_m = \frac{\int_{z_0}^{\infty} \frac{e}{T} dz}{\int_{z_0}^{\infty} \frac{e}{T^2} dz} \tag{11}$$

Thus, following [20], a relationship between T_m and the surface temperature T_s (K) is obtained through a linear fitting procedure between these two variables. Both T_m and T_s are obtained from the RAOBs data, the former deduced by (11). The linear fit for Milan (see Fig. 2) gives the following equation:

$$T_m = 88.04 + 0.66 T_{damped} \tag{12}$$

where:

$$T_{damped} = 0.25 T_s + 0.75 T_{ms} \tag{13}$$

and T_{ms} (K) is the daily mean surface air temperature. As proposed by Morland *et al*. [31], the use of a damped diurnal cycle, characterized by T_{damped} (K), allows the dependence of T_m on the diurnal variation of the surface temperature to be removed.

Estimates of T_m are obtained by (12) and (13) using T_s data from the weather station at PoliMi to test the procedure.

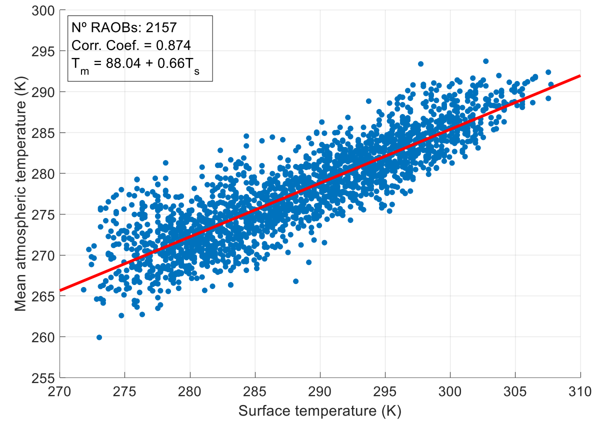

Fig. 2. Relationship between T_m and T_s from the analysis of RAOBs at Milano/Linate Airport (2014-2016). The solid red line represents the linear regression.

The zenith hydrostatic delay ZHD (mm) in (9), caused by the presence of well-mixed hydrostatic gases in the atmosphere, is modeled as a function of surface atmospheric pressure P_0 (hPa) [32]:

$$ZHD = \frac{2.2768 P_0}{1 - 0.00266 \cos(2\lambda) - 0.00028 H} \tag{14}$$

where λ (degrees) is the latitude, and H (km) is the height above the mean sea level. Due to the absence of local data for P_0 at the Como station, the measurements collected at PoliMi are used. However, it should be noted that there is a significant difference in height between Como and Milan (ΔH = 155 m), which prevents us from assuming that the atmospheric pressure at both sites is the same. Therefore, a height scaling factor k_p has to be used to estimate the ground atmospheric pressure at Como from that at Milan:

$$P_0 = k_p \ P_{0,Milan} \tag{15}$$

The value of k_p is derived using the mean annual global reference atmosphere model provided by the ITU-R [21]. In this model, the mean atmospheric pressure depends on the geopotential height h' (km), which is obtained from the geometric height h (km) by:

$$h' = \frac{6356.766 h}{6356.766 + h} \tag{16}$$

For each of the sites, Como and Milan, the conversion (15) is applied and then the atmospheric pressure $P(h')$ (hPa) is computed by:

$$P(h') = 1013.25 \left[\frac{288.15}{288.15 - 6.5 h'}\right]^{-34.1632/6.5} \tag{17}$$

At the end, k_p = 0.9797 is obtained as the ratio between the values of $P(h')$ calculated for Como and Milan.

B. Calculation of A_{dry} from Surface Temperature

The attenuation of dry air A_{dry}, given by the combined effect of oxygen plus the residual contribution of nitrogen, is

This article has been accepted for publication in a future issue of this journal, but has not been fully edited. Content may change prior to final publication. Citation information: DOI 10.1109/TIM.2019.2950612, IEEE Transactions on Instrumentation and Measurement

approximated as a linear function of T_s. To this aim, both variables are retrieved again from the RAOBs data as follow: A_{dry} calculated using the line-by-line method in Annex 1 of Recommendation ITU-R P.676-11 [29] both at 19.7 and 39.4 GHz, and T_s obtained as the temperature corresponding to the lowest layer of each vertical profile.

The linear fits of A_{dry} and T_s at both frequencies are shown in Fig. 3 and are given by:

$$A_{dry}(19.7) = (-2.637 \cdot T_s + 555) \cdot 10^{-4} \quad (18)$$

$$A_{dry}(39.4) = (-11.23 \cdot T_s + 2331) \cdot 10^{-4} \quad (19)$$

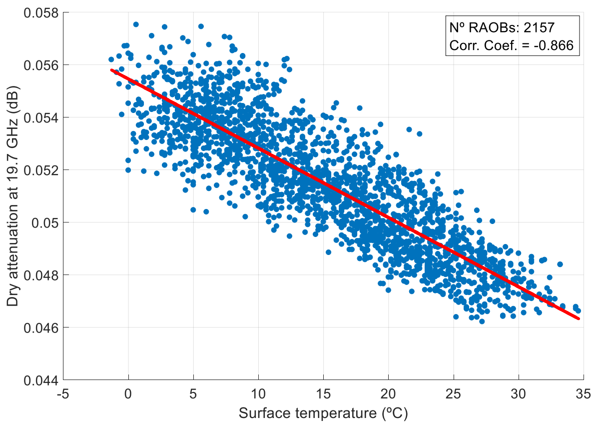

(a)

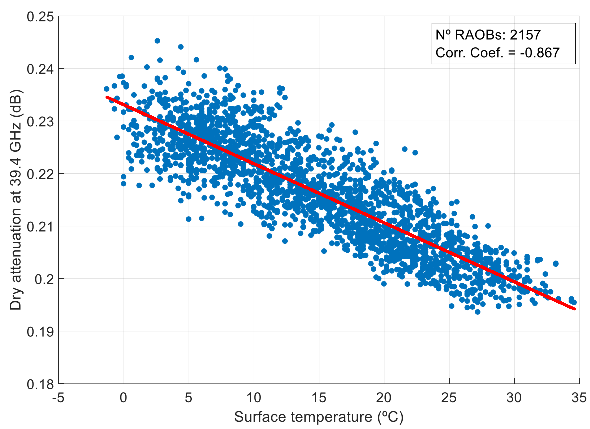

(b)

Fig. 3. Scatterplot of zenith dry-air attenuation versus surface temperature computed from the 2157 RAOBs at Milano Linate Airport (2014–2016) at the Alphasat beacon frequencies, (a) 19.7 GHz and (b) 39.4 GHz.

C. Calculation of A_g along the Slant Path

Gas attenuation A_g along the zenith path is easily computed as $A_g = A_{wv} + A_{dry}$, obtained from (7), (18) and (19). Slant path estimates of A_g, with an elevation angle φ = 35.42°, are calculated using the simple cosecant law, namely by dividing the zenithal attenuation by sin(φ). This approach assumes a horizontally stratified atmosphere model and is valid for angles of between 5° and 90° [29].

In short, the yearly time series of A_g at both frequencies are shown in Fig. 4. Missing data are due to outage periods of either the weather station or the GNSS receiver. It is a plausible assumption that these results can be used as estimates of A_g at PoliMi, because the EPN Como station and Milano Linate airport are both located in its proximities. P_{ref} is then computed on a daily basis using (5), interpolated during rain and cloud events, and A calculated by (6).

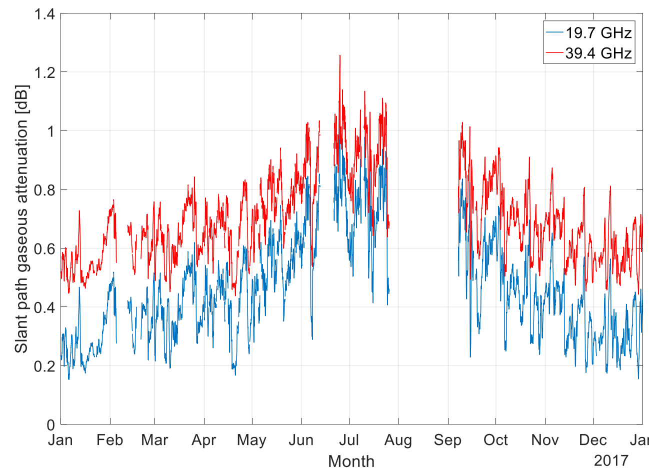

Fig. 4. Yearly time series of 1-hour slant path gaseous attenuation (φ = 35.42°) at the Alphasat beacon frequencies for PoliMi site, estimated using the UPM-UPB procedure.

V. PoliMi Procedure

The procedure developed by PoliMi aims to obtain A_g from the combination of vertical profiles of the troposphere, namely pressure (P), temperature (T) and relative humidity (RH), and mass absorption models.

For the specific case of the NASA receiver deployed in Milan, the *P-RH-T* profiles were obtained from the RAOBs data and from the ECMWF NWP products described in section II.C. These data are used as input to the line-by-line method in Annex 1 of Recommendation ITU-R P.676-11 [29] to calculate A_g from each set of *P-RH-T* profiles.

Given the coarse temporal resolution of the vertical profiles (6 hours, in the best case, for the ECMWF profiles), the procedure developed by PoliMi does not aim to produce a time series of A_g, as for the UPM-UPB procedure, but rather at finding a monthly average value for P_{ref} in (5) that can be used to derive the total tropospheric attenuation. In other words, the tropospheric attenuation A (dB) is obtained as:

$$A = \bar{P}_{ref} - P_r \quad (20)$$

where $\bar{P}_{ref}$ (dBm) is the monthly average value of $\bar{P}_{ref}(t^*)$, which, in turn, is calculated, for each vertical profile, as:

$$P_{ref}(t^*) = \bar{P}_r(t^*) + A_g(t^*) \quad (21)$$

$A_g(t^*)$ is the gas attenuation calculated using the line-by-line method in Annex 1 of Recommendation ITU-R P.676-11 [29] and the vertical profiles associated to the specific time instant t^*, while $\bar{P}_r(t^*)$ is the value of the received power averaged on a 10-minutes window around t^*.

This article has been accepted for publication in a future issue of this journal, but has not been fully edited. Content may change prior to final publication. Citation information: DOI 10.1109/TIM.2019.2950612, IEEE Transactions on Instrumentation and Measurement

The advantage of this approach is that no selection of rain/cloud attenuation events is required, but, on the other hand, only clear sky profiles must be included to calculate $P_{ref}(t^*)$ (and $\bar{P}_{ref}$), i.e. those for which $\bar{P}_r$ is only affected by gas attenuation. To this end, RAOBs profiles are first provided as input to the TKK (Teknillinen KorkeaKoulu) cloud detection method [33] to estimate the vertical distribution of the liquid water content *w* of the cloud and the ice water content *i*, while the same information on *w* and *i* is extracted directly from ECMWF NWP profiles. This is clarified in Fig. 5, which summarizes the full workflow to derive tropospheric attenuation from beacon measurements according to the PoliMi procedure: first, all the profiles collected during rain events (exploiting disdrometer data collected at PoliMi) are filtered out; secondly, profiles with any trace of *w* or *i* are also excluded.

Fig. 6 depicts $P_{ref}(t^*)$ for each set of vertical profiles of March 2017 (top side), along with the rain rate collected by the disdrometer (bottom side); as expected, a high variability in $P_{ref}(t^*)$ occurs during precipitation events (and to a lesser extent, in the presence of clouds) because $\bar{P}_r(t^*)$ is also affected by the attenuation caused by both rain and cloud particles. On the other hand, as shown in Fig. 7, $P_{ref}(t^*)$ is quite stable when only clear sky profiles are selected: the peak to peak variation of $P_{ref}(t^*)$ is approximately 0.3 dB (both bands). This corroborates the use of the monthly mean value of $P_{ref}(t^*)$, i.e. $\bar{P}_{ref}$ in (20), to calculate the tropospheric attenuation *A*, but it also highlights a limitation in the PoliMi procedure: the accuracy of the method depends on the stability of $P_{ref}(t^*)$ through the month, which, in turn, is linked to the amount of receiver-induced effects such as changes in the *EIRP* and, more commonly, in the receiver gain chain as a function of temperature.

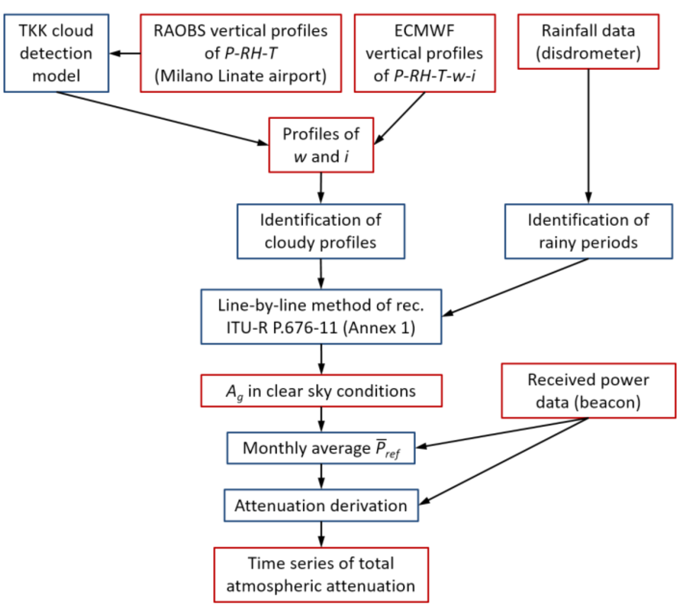

Fig. 5. Detailed workflow for the derivation of tropospheric attenuation using RAOBs and ECMWF NWP data. Red boxes refer to data, while blue ones to models or procedure.

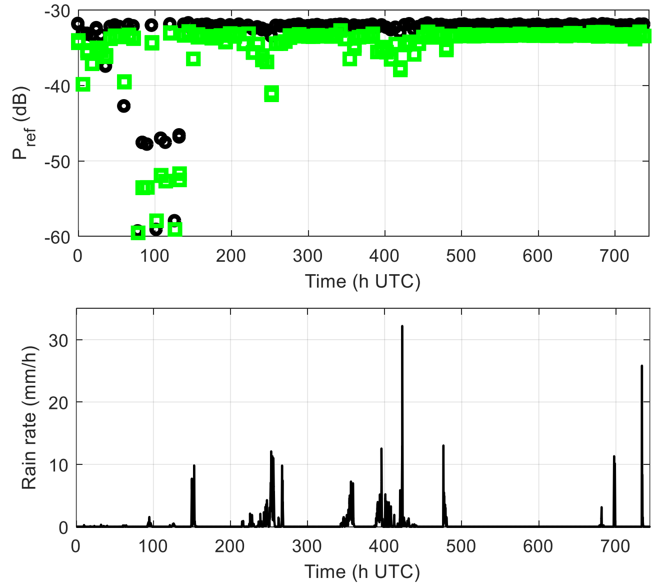

Fig. 6. $P_{ref}(t^*)$ at Ka band (black circles) and Q band (green squares) for each set of vertical profiles of March 2017 (at the top), along with the rain rate collected by the disdrometer collocated with the Alphasat beacon receivers (at the bottom).

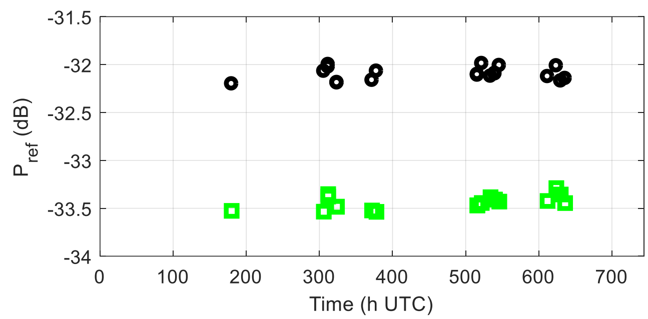

Fig. 7. $P_{ref}(t^*)$ at Ka band (black circles) and Q band (green squares) only for the clear sky vertical profiles of March 2017, using RAOBS and ECMWF profiles.

When no local vertical atmospheric profiles are available, neither from RAOBS nor from ECMWF, the PoliMi procedure can still be applied by resorting the standard atmospheric profiles adopted by the ITU-R (International Telecommunication Union – Radiocommunication Sector) in recommendation P.835-6 [21], which defines single seasonal average profiles of *P*, *T* together with the water vapor content ρ. For the site of Milan, we have selected the standard profiles defined as “winter mid-latitude” and “summer mid-latitude”: the latter is assumed to be valid from April to September, while the former is associated to the remaining months.

Fig. 8 shows the same information as in Fig. 7, but using the standard atmospheric profiles for every 6-hour slot instead of those extracted from RAOBS and ECMWF data: $\bar{P}_{ref}$ changes from -32.1 dB to -31.7 dB for the Ka band, and from -33.4 dB to -33.1 dB for the Q band. Note that Fig. 8 contains fewer points than Fig. 7, as RAOBS data are not considered. It should also be mentioned that the standard atmospheric

This article has been accepted for publication in a future issue of this journal, but has not been fully edited. Content may change prior to final publication. Citation information: DOI 10.1109/TIM.2019.2950612, IEEE Transactions on Instrumentation and Measurement

profiles provide no information on the possible presence of clouds: in Fig. 8, for the sake of a proper comparison, the selection of clear sky days was made in the same way as in Fig. 7 (i.e. by relying on the ECMWF profiles of *w* and *i*); in a more general case, i.e. when only standard atmospheric profiles are actually used, the selection can be achieved by looking for $P_{ref}(t^*)$ values not deviating significantly from baseline levels, to be identified through a visual inspection of all $P_{ref}(t^*)$ values (see Fig. 6).

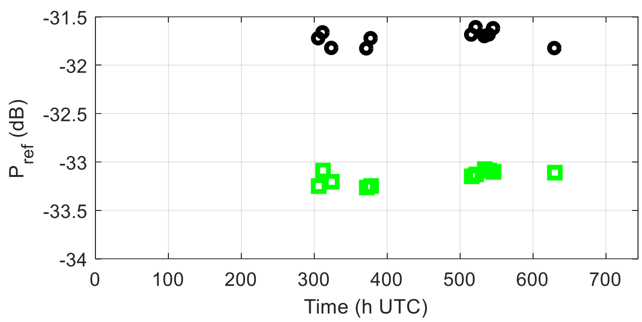

Fig. 8. $P_{ref}(t^*)$ at Ka band (black circles) and Q band (green squares) only for clear sky vertical profiles of March 2017, using standard atmospheric profiles.

Overall, the maximum absolute difference in $\bar{P}_{ref}$ due to using RAOBS+ECMWF profiles or standard profiles is obtained in April (0.4 dB and 0.42 dB for Ka band and Q band, respectively), while the minimum one is associated to February (0.1 dB both bands).

VI. Assessment of the Accuracy of the Procedures

As already mentioned in Section III, the most accurate way of deriving tropospheric attenuation from beacon power data is to use a radiometer collocated with the beacon receiver by applying equation (4) [17]. Let A_{MWR}, $A_{UPM\text{-}UPB}$ and A_{PoliMi} denote the tropospheric attenuation derived with the support of radiometric data (according to the well-established procedure fully described in [18], which consists in inverting brightness temperatures data to estimate the tropospheric attenuation – see also [34] and [20]), and obtained by applying the UPM-UPB procedure (Section IV) and that developed by PoliMi (Section V), respectively, whose accuracy is evaluated by using the following error figure $\varepsilon_i(t)$:

$$\varepsilon(t) = A(t) - A_{MWR}(t) \quad (22)$$

In (22), $A(t)$ is the attenuation derived using either of the procedures.

Fig. 9 and Fig. 10 report the trend, on a daily basis, of the average value, *E* (top), and of the root mean square value, *RMS* (bottom), of the error figure ε (Ka band and Q band, respectively, for the whole of 2017), which are used to quantify and compare the performance of the three procedures. Note that the figure includes results from the PoliMi procedure obtained using RAOBS+ECMWF profiles (label 'PoliMi') and standard atmospheric profiles (label 'PoliMi (STD)'). The missing data in the plots correspond to days when GPS data and/or radiometric data were not available; notably, the quite large discontinuity in the data, covering the last days of July, the whole of August and the first half of September, is due to the absence of the radiometer, which was under repair.

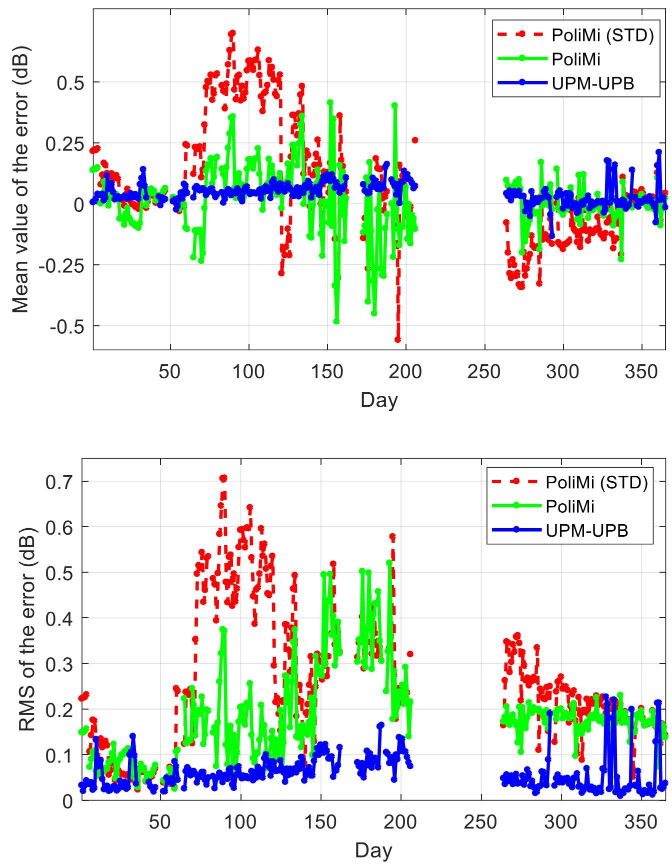

Fig. 9. Trend of the daily mean (*E*) and root mean square (*RMS*) values of the error figure ε for the whole of 2017 at the Ka band.

Overall, the results in Fig. 9 and Fig. 10 indicate that the accuracy of the UPM-UPB procedure is higher than that of the PoliMi procedure, which, as expected, worsens even more when standard profiles are used as input instead of the RAOBS+ECMWF profiles; moreover, while the error associated to the UPM-UPB procedure is more stable throughout the year, the *RMS* of the PoliMi procedure is higher during the Spring and Summer, with few peaks reaching 0.5 dB and 1 dB at the Ka band and Q band, respectively, using RAOBS+ECMWF profiles as input. In a few cases, these *RMS* peaks increase even more for the PoliMi procedure using standard profiles, as they reach almost 1 dB and 1.5 dB, at the Ka band and Q band, respectively.

The more limited accuracy of the PoliMi procedure is mainly dependent on the fluctuation of the received power due to the variation in the internal temperature of the receiver, which, in turn, induces a change in the overall gain in the receiver chain, as well as an oscillation in the noise floor. As a consequence of using a monthly average value of $\bar{P}_{ref}$, the PoliMi procedure does not allow to compensate for these receiver-induced oscillations in the signal. This effect is

This article has been accepted for publication in a future issue of this journal, but has not been fully edited. Content may change prior to final publication. Citation information: DOI 10.1109/TIM.2019.2950612, IEEE Transactions on Instrumentation and Measurement

clearly visible in Fig. 11, which details the tropospheric attenuation at the Ka band collected on the 12th of July 2017 (top side), i.e. the day associated with the highest *RMS* (0.52 dB) for the PoliMi in this band (RAOBS+ECMWF profiles). The trend of A_{PoliMi} and of the air temperature, measured by the sensor collocated with the radiometer (at the bottom of Fig. 11), are very similar (using both types of profile as inputs). Also reported as a reference in Fig. 11 is A_{MWR}, which indicates very stable weather conditions during a typical clear sky day. The rapid variations in the signal (scintillations) are due to turbulence in the troposphere.

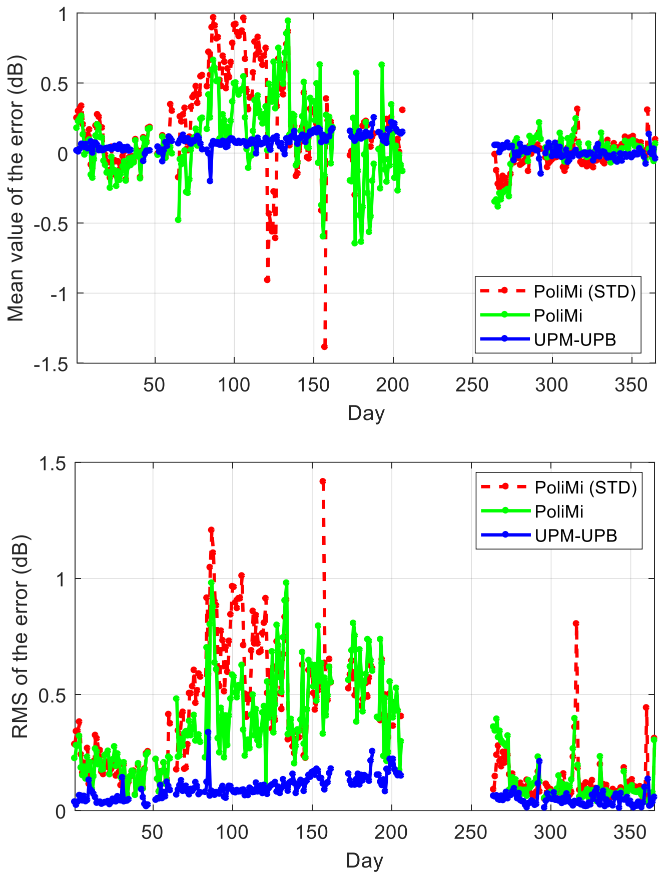

Fig. 10. Trend of the daily mean (E) and root mean square (*RMS*) values of the error figure ε for the whole of 2017 at the Q band.

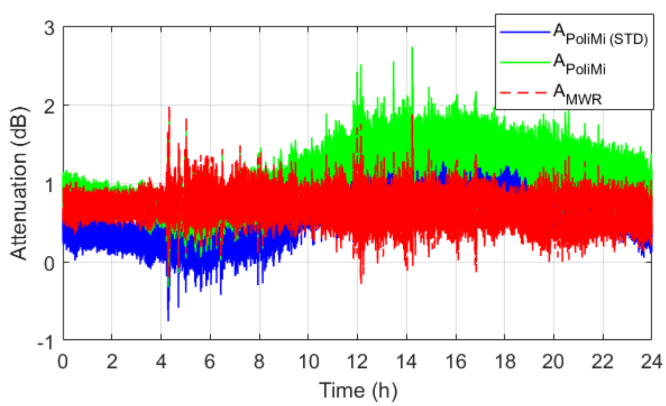

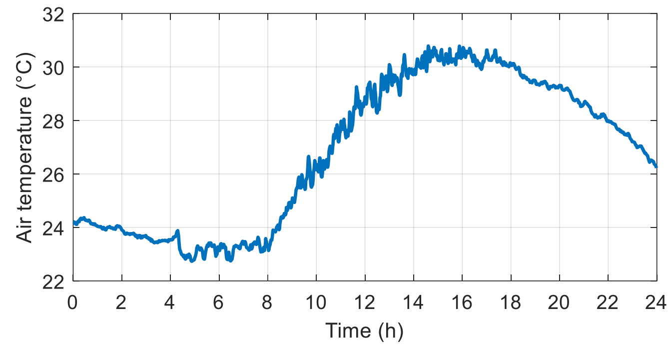

Fig. 11. Tropospheric attenuation at the Ka band (top) and ground air temperature (bottom) on 12th of July 2017.

The impact of the internal temperature of the receiver on the effectiveness of the PoliMi procedure is confirmed by the lowest *RMS* values obtained in the last part of the year, after repairing both the controller and the fan in charge of stabilizing the temperature inside the box where the radio frequency (GHz) is downconverted to the intermediate frequency (MHz) before sampling the signal. The improvement is reflected in the results shown in Fig. 12 (for both types of profile), which shows a good agreement between A_{MWR} and the profile-derived attenuations (26th of November 2017, Q-band signal, *RMS* = 0.06 dB for A_{PoliMi}), notwithstanding a non-negligible excursion in the air temperature during the day. It is worth pointing out that, for this specific day, the difference between using RAOBS+ECMWF profiles and standard atmospheric ones is negligible.

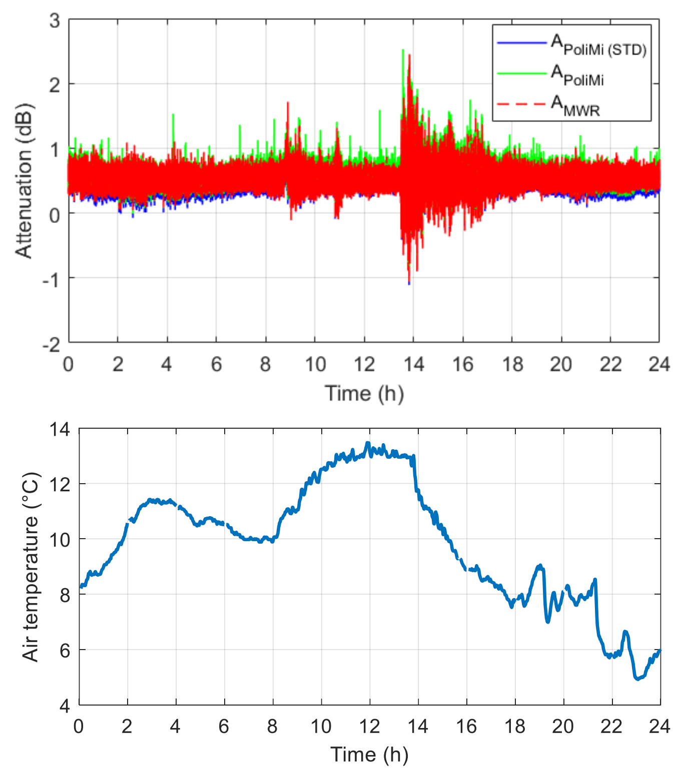

Fig. 12. Tropospheric attenuation at the Q band (top) and ground air temperature (bottom) on 26th of November 2017.

This article has been accepted for publication in a future issue of this journal, but has not been fully edited. Content may change prior to final publication. Citation information: DOI 10.1109/TIM.2019.2950612, IEEE Transactions on Instrumentation and Measurement

In contrast with the results achieved by the PoliMi procedure, the performance of the UPM-UPB method is more stable and independent of the system-induced oscillations of the received power. The availability of the reference gaseous attenuation at high temporal resolution allows the compensation for such variations in the signal, thus achieving maximum *RMS* values of around 0.2 dB and 0.35 dB for the Ka band and the Q band, respectively (see Fig. 9 and Fig. 10). As an example, Fig. 13 shows the comparison between $A_{UPM\text{-}UPB}$ and A_{MWR} (Ka band) for the 24th of November 2017, i.e. the day for which the UPM-UPB procedure provides the largest *RMS* (0.22 dB). The discrepancy is likely to be mostly ascribable to the difficulty in identifying rain (and cloud) events correctly, which is a necessary step in the UPM-UPB procedure, as explained in Section III. Indeed, this is not always an easy task; in the example reported in Fig. 13, the inspection of the rain rate derived from the disdrometer is not sufficient to fully identify the presence of rain throughout the link, whose impact is clearly visible from the trend of A_{MWR} also of around 12 and 18 UTC, as well as obviously from 20 UTC on, as indicated by the disdrometer.

For the sake of completeness, Fig. 14 compares $A_{UPM\text{-}UPB}$ and A_{MWR} at the Q band collected on the 26th of March 2017, the day associated with the highest *RMS* (0.35 dB) as obtained by applying the UPM-UPB procedure. The hole in the data is due to a temporary failure of the beacon receiver during that particular day.

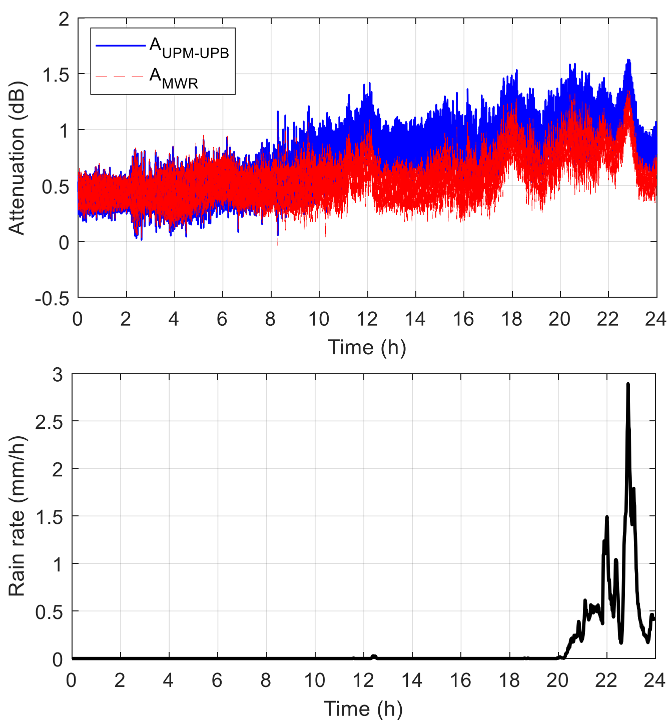

Fig. 13. Tropospheric attenuation at the Ka band (top) and rain rate (bottom) on 24th of November 2017.

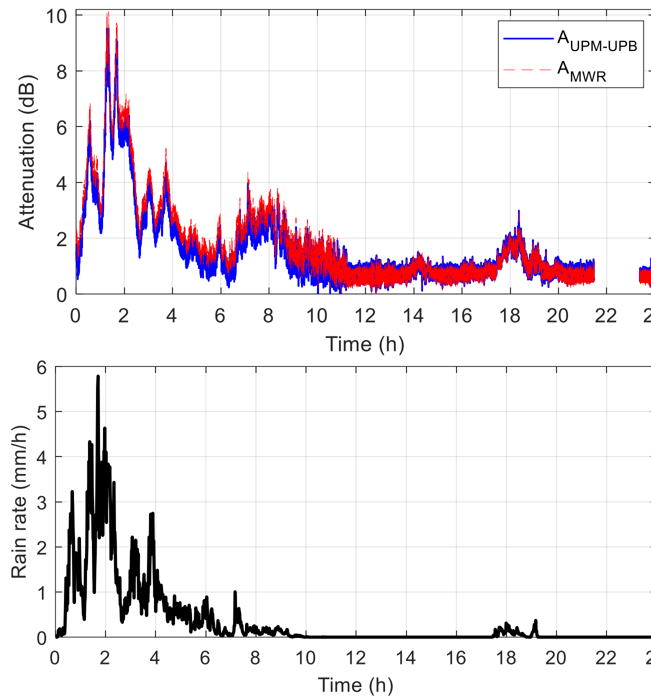

Fig. 14. Tropospheric attenuation at the Q band (top) and rain rate (bottom) on 26th of March 2017.

Fig. 15 and Fig. 16 complete the evaluation of the accuracy of the procedures by comparing the Complementary Cumulative Distribution Functions (CCDFs) of $A_{UPM\text{-}UPB}$, A_{PoliMi} and A_{MWR}, at the Ka band and Q band, respectively. The statistical results confirm that the application of the PoliMi procedure using the standard atmospheric profiles as input leads to a higher error. On the other hand, when the latter results are excluded, there is almost no difference between the remaining three curves at the Ka band, while the highest accuracy of the UPM-UPB procedure emerges at the Q band.

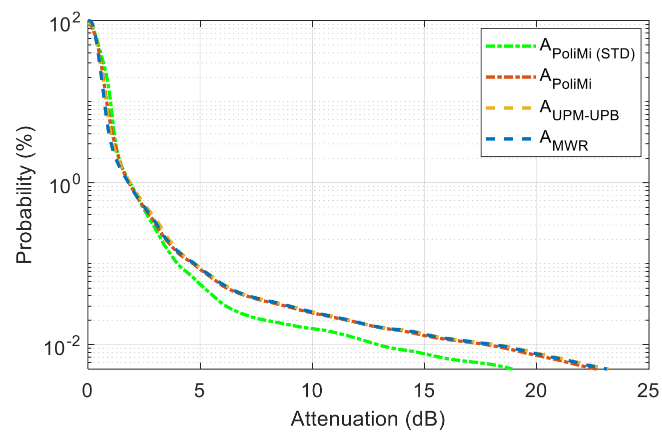

Fig. 15. Yearly CCDF of the tropospheric attenuation for 2017 at the Ka band.

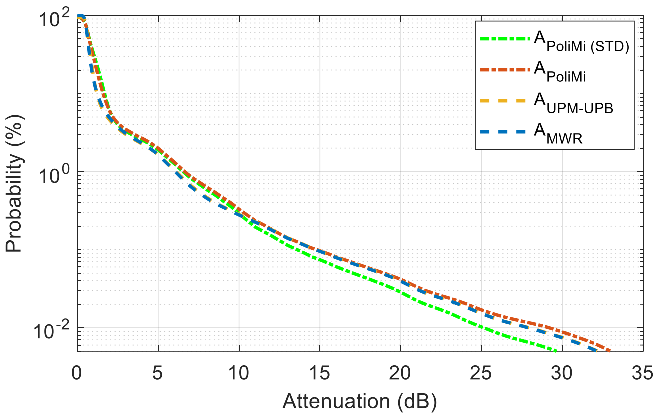

Fig. 16. Yearly CCDF of the tropospheric attenuation for 2017 at the Q band.

VII. Conclusions

This paper presents three procedures to estimate gas attenuation and its use to derive tropospheric attenuation from the raw power data received on the ground by beacon receivers within the framework of satellite propagation experiments. These estimates of gas attenuation, namely water vapor and oxygen contributions, are used as the reference baseline attenuation level under clear sky conditions. The three methodologies make use of different ancillary data: a) GNSS-derived measurements, vertical atmospheric profiles extracted from RAOBs and surface meteorological data for the UPM-UPB procedure; b) profiles of pressure, temperature and relative humidity extracted from RAOBs + NWP products, or c) derived from standard atmospheric profiles for the PoliMi procedure. The use of any of these procedures can be an alternative to the use of a radiometer, since the latter is an expensive piece of equipment that is not always available in the context of propagation experiments.

The procedures are tested against a full year of tropospheric attenuation time series obtained by combining beacon power data and radiometric brightness temperature measurements, collected in Milan in 2017 within the framework of the Alphasat Aldo Paraboni propagation experiment. These attenuation time series are considered as the reference. The aim of the comparison is to evaluate the degradation that may arise from the use of the three alternative procedures.

The results indicate that, overall, the UPM-UPB procedure offers more accurate results (average *RMS* of the error equal to 0.06 dB and 0.08 dB, for the Ka band and the Q band, respectively, with peak daily values of around 0.2 dB and 0.35 dB, for the two bands) by taking advantage of the better temporal resolution of GNSS data; on the other hand, it needs more ancillary data as input (together with GNSS-derived water vapor data, long-term full vertical profiles of the atmosphere and surface meteorological data) and it is also a more complex application because the manual selection of cloud and rain attenuation events requires know-how from an expert operator. As for the PoliMi procedure, it is easier to apply (no selection of cloud/rain events on the received power time series is needed) and it makes use of less input data (just vertical atmospheric profiles extracted from RAOBS and/or NWP data), but this comes at the expense of a slightly worse performance (average *RMS* of the error equal to 0.19 dB and 0.31 dB, for the Ka band and the Q band, respectively, with peak daily values of around 0.5 dB and 1 dB, for the two bands). When no local vertical profiles are available, the PoliMi procedure can still be applied using the ITU-R standard atmospheric profiles as input, though with a further decrease in the accuracy (average *RMS* of the error equal to 0.27 dB and 0.38 dB, for the Ka band and the Q band, respectively, with peak daily values reaching almost 1 dB and 1.5 dB, for the two bands). In principle, the three procedures can be applied on a Global basis, but additional validation of their accuracy in other climatic regions should be performed using beacon measurements collected, for example, in tropical/equatorial sites.

Overall, results show that all the procedures considered in this work are useful and can be equally recommended, their use being mainly conditioned to the availability of the appropriate data in the area around the experimental site (e.g. GNSS receivers or RAOBS profiles). These new procedures can be implemented by experimenters as an alternative to the use of multichannel radiometers in satellite propagation experiments.

Acknowledgment

The authors would like to thank the EUREF Permanent GNSS Network for providing ZTD data from Como Station as well as Ms. Rosa Pacione who provided insights about this database. Moreover, the authors would like to thank ECMWF for producing vertical atmospheric profiles.

References

[1] D. Minoli, “Innovations in satellite communications and satellite technology,” in High Throughput Satellites (HTS) and Ka/Ku Spot Beam Technologies. Hoboken, NJ, USA: Wiley, 2015, ch. 3.

[2] T. Rossi, M. De Sanctis, F. Maggio, M. Ruggieri, G. Codispoti and G. Parca, “Analysis of satellite Q/V band channel errors based on Italian experimental campaign,” 2017 IEEE Aerospace Conference, Big Sky, MT, 2017, pp. 1-9.

[3] A. Costouri, “European W-Band Propagation Campaign Development,” 2018 12th European Conference on Antennas and Propagation (EuCAP), London, UK, 9-13 April 2018, pp. 1-5.

[4] F. Machado, P. Mariño, F. Poza, M. A. Domínguez and F. P. Fontán, “FPGA-Based Instrument for Satellite Beacon Monitoring on Propagation Experiments,” in IEEE Transactions on Instrumentation and Measurement, vol. 63, no. 12, pp. 2761-2770, Dec. 2014.

[5] J. A. Nessel, M. J. Zemba and J. R. Morse, “Design of a K/Q-band beacon receiver for the Alphasat TDP#5 experiment,” 2014 IEEE Antennas and Propagation Society International Symposium (APSURSI), Memphis, TN, 2014, pp. 263-264.

[6] B. R. Arbesser-Rastburg, A. Paraboni, “European research on Ka-band slant path propagation,” Proceedings of the IEEE, vol. 85, no. 6, pp. 843 - 852, June 1997.

[7] F. Carducci, M. Francesi, “The Italsat satellite system,” International Journal of Satellite Communication and Networking, vol. 13, no. 1, pp. 49-81, 1995.

[8] R. K. Crane, X. Wang; D. B. Westenhaver; W. J. Vogel, “ACTS propagation experiment: experiment design, calibration, and data preparation and archival,” Proceedings of the IEEE, vol. 85, no. 6, pp, 863 - 878, June 1997.

This article has been accepted for publication in a future issue of this journal, but has not been fully edited. Content may change prior to final publication. Citation information: DOI 10.1109/TIM.2019.2950612, IEEE Transactions on Instrumentation and Measurement

[9] O. Koudelka, “Q/V-band communications and propagation experiments using ALPHASAT,” Acta Astronautica, vol. 69, no. 11-12, pp. 1029-1037, 2011.

[10] T. Rossi, M. De Sanctis, M. Ruggieri, C. Riva, L. Luini, G. Codispoti, E. Russo, G. Parca, “Satellite communication and propagation experiments through the Alphasat Q/V band Aldo Paraboni technology demonstration payload,” IEEE Aerospace and Electronic Systems Magazine, vol. 31, no. 3, pp. 18-27, March 2016.

[11] ESA ITT, “Cubesat-based W-band channel measurement,” 2017.

[12] P. Mariño, F. Machado, F. P. Fontan and S. Otero, “Hybrid Distributed Instrumentation Network for Integrating Meteorological Sensors Applied to Modeling RF Propagation Impairments,” in IEEE Transactions on Instrumentation and Measurement, vol. 57, no. 7, pp. 1410-1421, July 2008.

[13] F. Davarian, “An Update on NASA Ka-Band Propagation Measurements,” IEEE Antennas & Propagation Magazine, vol. 36, no. 3, pp. 14-18, June 1994.

[14] J. M. Riera, K. Al-Ansari, P. Garcia, J. L. Besada, “Low-cost millimeter-wave beacon receiver including total-power radiometer: design implementation and measurement calibration,” Antennas and Propagation Magazine IEEE, vol. 44, no. 1, pp. 45-54, 2002.

[15] R. Bleisch, N. Kämpfer, and A. Haefele, “Retrieval of tropospheric water vapour by using spectra of a 22 GHz radiometer,” Atmospheric Measurement Technique, vol. 4, pp. 1891–1903, 2011.

[16] M.P. Cadeddu, J.C. Liljegren, and D.D. Turner, “The Atmospheric radiation measurement (ARM) program network of microwave radiometers: instrumentation, data, and retrievals,” Atmospheric Measurement Techniques, vol. 6, pp. 2359-2372, 2013.

[17] L. Luini, C. Riva, C. Capsoni and A. Martellucci, “Attenuation in Nonrainy Conditions at Millimeter Wavelengths: Assessment of a Procedure,” in IEEE Transactions on Geoscience and Remote Sensing, vol. 45, no. 7, pp. 2150-2157, July 2007.

[18] L. Luini, C. Riva, R. Nebuloni, M. Mauri, J. Nessel, A. Fanti, “Calibration and Use of Microwave Radiometers in Multiple-site EM Wave Propagation Experiments,” EuCAP 2018, 9-13 April 2018, London, UK.

[19] E. Fionda, V. Mattioli, P. Ciotti, “GNSS radio-path delay: Tool to assess satellite channels water vapour’s attenuation,” in COST Action IC0802 Handbook of Microwave Propagation Measurements for Satellite and Terrestrial Links, to be published.

[20] G. A. Siles, J. M. Riera and P. García-del-Pino, “An Application of IGS Zenith Tropospheric Delay Data to Propagation Studies: Validation of Radiometric Atmospheric Attenuation,” IEEE Transactions on Antennas and Propagation, vol. 64, no. 1, pp. 262-270, Jan. 2016.

[21] ITU-R, “Reference Standard Atmospheres,” ITU-R Recommendation P. 835-6, 2017.

[22] EUREF Permanent GNSS Network European. Accessed Feb. 2019. [Online]. Available: http://www.epncb.oma.be.

[23] R. Pacione, A. Araszkiewicz, E. Brockmann E, J. Dousa, “EPN-Repro2: a reference GNSS tropospheric data set over Europe,” Atmospheric Measurement Techniques. vol. 10, no. 5, pp. 1689–1705, 2017.

[24] EUREF Permanent GNSS Network Server. Accessed Feb. 2019. [Online]. https://igs.bkg.bund.de/root_ftp/EUREF/products/.

[25] J. M. Riera, G. A. Siles, P. Garcia-del-Pino and A. Benarroch, “Alphasat propagation experiment in Madrid: Processing of the first year of measurements,” 2016 10th European Conference on Antennas and Propagation (EuCAP), Davos, Switzerland, 10-15 April 2016, pp. 1-5.

[26] M. Bevis, S. Businger, T. A. Herring, C. Rocken, R. A. Anthes, R. H. Ware, “GPS meteorology: Remote sensing of atmospheric water vapor using the global positioning system,” J. Geophys. Res., vol. 97, no. D14, pp. 15787–15801, 1992.

[27] G. Guerova, J. Jones, J. Douša, G. Dick, S. de Haan, E. Pottiaux, O. Bock, R. Pacione, G. Elgered, H. Vedel, and M. Bender, “Review of the state of the art and future prospects of the ground-based GNSS meteorology in Europe,” Atmospheric Measurement Techniques, vol. 9, pp. 5385-5406, 2016.

[28] T. Ning, J. Wang, G. Elgered, G. Dick, J. Wickert, M. Bradke, M. Sommer, R. Querel, and D. Smale, “The uncertainty of the atmospheric integrated water vapour estimated from GNSS observations,” Atmospheric Measurement Techniques, vol. 9, pp. 79-92, 2016.

[29] ITU-R, “Attenuation by atmospheric gases,” ITU-R Recommendation P. 676-11, 2017.

[30] J. M. Rüeger, “Refractive Index Formulae for Radio Waves,” JS28 Integration of Techniques and Corrections to Achieve Accurate Engineering, FIG XXII International Congress, Washington, 2002.

[31] J. Morland, M. Collaud Coen, K. Hocke, P. Jeannet, C. Mätzler, “Tropospheric water vapour above Switzerland over the last 12 years,” Atmos. Chem. Phys., vol. 9, no. 16, pp. 5975–5988, 200.

[32] J. L. Davis, T. A. Herring, I. I. Shapiro, A. E. E. Rogers, G. Elgered, “Geodesy by radio interferometry: Effects of atmospheric modeling errors on estimates of baseline length,” Radio Sci., vol. 20, no. 6, pp. 1593–1607, 1985.

[33] E. Salonen, S. Uppala, “New prediction method of cloud attenuation,” Electron. Lett., vol. 27, no. 12, pp. 1106–1108, Jun. 1991.

[34] X. Boulanger, B. Gabard, L. Casadebaig and L. Castanet, “Four Years of Total Attenuation Statistics of Earth-Space Propagation Experiments at Ka-Band in Toulouse,” *IEEE Transactions on Antennas and Propagation*, vol. 63, no. 5, pp. 2203-2214, May 2015.